J. Fluid Mech. (1996), *vol.* 316, *pp.* 163–172

Oblique wind waves generated by the instability of wind blowing over water

By L. C. MORLAND

Department of Mathematics, Southern Methodist University, Dallas, TX 75275, USA

(Received 26 January 1994 and in revised form 26 June 1995)

The growth rates of gravity waves are computed from linear, inviscid stability theory for wind velocity profiles that are representative of the mean flow in a turbulent boundary layer. The energy transfer to the waves is largely concentrated in an angle (to the wind) interval that broadens with increasing wind speed and narrows with increasing wavelength. At sufficiently high wind speeds and sufficiently short wavelengths, the waves of maximum growth rate propagate at an oblique angle to the wind. The connection with bimodal directional distributions of observed spectra is discussed.

1. Introduction

In a paper concerning the instability of wind blowing over water, Morland & Saffman (1993) described a Squire's transformation that relates the linear growth rate of an oblique gravity wave to that of a wave propagating in the direction of the wind. They noted that for logarithmic wind profiles, representative of the mean flow in a turbulent boundary layer, Squires's theorem does not hold, i.e. the wave of maximum growth rate does not necessarily propagate in the wind direction. In this paper, the growth rates of oblique waves are examined in detail, and their influence on the directional distributions of gravity wave spectra is discussed.

The inviscid instability studied here is caused by the critical-layer mechanism for the transfer of energy from the wind to the waves, discovered by Miles (1957). For a given logarithmic profile, it acts on waves whose critical layers lie above the viscous sublayer. As can be seen in figure 4 of Morland & Saffman, the growth rate decreases rapidly to zero with decreasing wavelength, once the critical layer has descended into the viscous sublayer. Although stable, or nearly stable, according to inviscid theory, waves whose critical layers lie in the viscous sublayer are subject to a viscous instability (Benjamin 1959; Miles 1962), and for these waves the inviscid instability appears to be unimportant physically. Hence, attention is focused on waves whose critical layers lie above the viscous sublayer, i.e. waves for which $c \gg u_*$, where c is the phase speed of the wave and u_* is the friction velocity of the mean flow.

The approach to studying the instability adopted here, numerical solution of Rayleigh's equation, can be extended to include viscosity by replacing the Rayleigh equation by the Orr–Sommerfeld equation, as was done by Valenzuela (1976) in the case of waves aligned with the wind. However, the Orr–Sommerfeld equation requires an additional asymptotic boundary condition at large heights above the water surface, which in the case of logarithmic profiles, cannot be found in closed form, and hence is an additional source of uncertainty in the calculation.

In the critical-layer theory, the presence of turbulence is taken into account in the choice of basic state, but the perturbed Reynolds stresses are neglected in the linearized equations. In order to include these terms, a turbulence model is required. Van Duin & Janssen (1992), building on the work of Jacobs (1987) (see also Knight 1977), use a family of first-order closure models to develop an asymptotic theory of wave generation in the limit of small ratio of friction velocity to wind speed. They derive a formula for the growth rate, which depends on the choice of turbulence model. In their analysis, the contribution to the growth rate from the critical-layer mechanism is negligible compared to the contribution from the perturbed Reynolds stresses. However, Miles (1993) finds that the two contributions are similar in magnitude. Belcher & Hunt (1993) use a truncated mixing-length turbulence model. They find that the dominant contribution to the growth rate is due to a non-separated sheltering mechanism and so, as in van Duin & Janssen's analysis, the critical-layer mechanism does not contribute at leading order. However, their growth rates are, asymptotically, an order of magnitude smaller than those of van Duin & Janssen. Hence at present, the relative importance of the critical-layer mechanism is an unresolved issue.

The results presented here, for wind speeds and wavelengths typical of those in field observations, show that at fixed wavelength and wind speed, positive growth rates, and hence energy input from the wind, occur in an azimuthal angle interval centred on the wind direction. In fact, the growth rate is positive for all angles in $(-\pi/2, \pi/2)$, but as will be seen in §4, there is a well-defined interval of positive growth rate, outside which growth rates are negligible. The width of the interval decreases with increasing wavelength and increases with increasing wind speed. The interval of positive growth rate is in good agreement with the corresponding intervals given by the formula of Snyder *et al.* (1981) that summarizes field data and by van Duin & Janssens' formula for oblique waves. Although there is good agreement in the interval of positive growth rate, there is in general a discrepancy between the growth rates from the three sources; especially between the theoretical and observational growth rates. Van Duin & Janssen note that their formula underestimates the observed growth rates, and the same is true of the growth rates presented here, which are of the same order of magnitude as those computed by van Duin & Janssen. In contrast with the inviscid instability, van Duin & Janssen predict negative growth rates, i.e. damping, outside the interval of positive growth rate.

The summary of field observations, van Duin & Janssens' formula, and the numerical boundary-layer model of Burgers & Makin (1993) give only single-peaked growth rates, while the inviscid critical-layer mechanism and Phillips' resonant wave generation mechanism (Phillips 1957) can produce double-peaked growth rates. The relationship between the energy transfer from the wind to waves and an observed wave spectrum is indirect, because of energy dissipation by wave breaking, wave–wave interactions, and wave scattering by subsurface currents. The relationship is complicated further by the flow separation that accompanies wave breaking (Banner & Melville 1976). These mechanisms, with the exception of wave scattering, which has not been studied extensively, are discussed by Phillips (1977).

Wave scattering by subsurface currents and its influence on gravity wave spectra was first examined in detail by Zakharov & Shrira (1990). Their work was motivated, in part, by the need to explain why the directional distributions of the spectra of gravity waves observed at sea (Mitsuyasu *et al.* 1975; Donelan, Hamilton & Hui 1985) were narrower than expected, given the broadening influence of wave–wave interactions. They concluded that wave scattering acts to narrow the angular spectrum, but to

such an extent that, when it is taken into consideration, the spectra at sea appear to be too broad.

Bimodal directional distributions have been observed in the field. (At a given frequency f, the directional distribution is $h(\theta) = F(f, \theta)$, or a normalization of h, where θ is the angle to the wind and F is the directional spectrum.) Phillips (1958) examined the connection between bimodal directional distributions from the SWOP data (Coté *et al.* 1960) and his resonant wave generation theory. More recently, the ROWS spectrum obtained by Jackson, Walton & Peng (1985) was found to be very similar to the SWOP spectrum, including the occurrence of bimodal structures, and it was concluded that the results supported the action of the resonance mechanism (see also Phillips 1988.)

The SWOP and ROWS spectra were obtained under conditions of large fetch. Under fetch-limited conditions, bimodal directional distributions were observed to occur occasionally by Donelan *et al.* and are a general feature of the spectra of Young, Verhagen & Banner (1995). Young *et al.* found that bimodal directional distributions occur when the frequency is greater than a value that is approximately twice the peak frequency and note that the data of Donelan *et al.* extend only to 1.6 times the peak frequency.

Two energy transfer mechanisms, the critical-layer mechanism and Phillips' resonance mechanism, would in isolation lead to bimodal directional distributions. However, the dissipation mechanisms may also be responsible for bimodal directional distributions. Zakharov & Shrira find that wave scattering generally gives rise to bimodal directional spectra, and it has been suggested (Jackson *et al.*) that wave–wave interactions may also be responsible for producing bimodal directional distributions. Young *et al.* compare the results of a numerical model with their experimental data, and the comparison indicates that the bimodal distributions are maintained by energy transfer through wave–wave interactions.

In §2 the linear theory is developed, in §3 the occurrence of double-peaked growth rates is interpreted in terms of Squire's transformation, and in §4 the results are presented. At a fixed wind speed, the growth rate is found to be a double-peaked function of angle to the wind for sufficiently short waves. The cases presented in detail satisfy the condition described above, $c \gg u_*$, but in addition, they satisfy the more stringent condition that the growth rates are insensitive to the form of the wind near to the water surface. This condition has been verified by using four families of basic states, each of which tends with increasing height to the logarithmic profile of the mean flow of a turbulent boundary layer, but which differ in treatment of the viscous sublayer. When this second condition is imposed, it is only at the higher wind speeds that double-peaked growth rates are unambiguously predicted. The results are summarized in §5.

2. Linear theory

A right-handed Cartesian coordinate system is defined in which the origin is at the mean level of the water surface, the x-axis points in the direction of the wind, and the y-axis points vertically upwards. In the basic state a planar interface separates quiescent water from air in plane, parallel motion, with velocity given by $\boldsymbol{u} = (U(y), 0, 0)$. The governing equations in both fluids are the Euler equations and the equation of mass conservation. At the interface the boundary conditions are continuity of pressure and the kinematic condition, and at large distances from the interface the velocity is required to tend to that of the basic state.

Following the standard procedure, the linearized equations for perturbations to the basic state, proportional to $\exp[\mathrm{i}(\alpha x + \beta z - \omega t)]$, are derived. The equations are simplified by applying a Squire's transformation to produce an associated two-dimensional problem with wavenumber $\tilde{\alpha} = (\alpha^2 + \beta^2)^{1/2}$, velocity eigenfunctions $\tilde{u} = (\alpha u + \beta v)/\tilde{\alpha}$ and $\tilde{v} = v$, angular frequency $\tilde{\omega} = \tilde{\alpha}\omega/\alpha$, and gravity $\tilde{g} = (\tilde{\alpha}/\alpha)^2 g$. The transformation yields an eigenvalue problem for the wave speed of the associated two-dimensional perturbation, $c = \tilde{\omega}/\tilde{\alpha} = \omega/\alpha$. The absence of vorticity in the basic state of the water allows the eigenfunctions to be found analytically in $y < 0$, leaving the eigenfunctions to be determined in $y > 0$,

$$\tilde{v}_{yy} - \left(\tilde{\alpha}^2 + \frac{U_{yy}}{U - c}\right)\tilde{v} = 0, \qquad 0 < y < \infty, \tag{2.1a}$$

$$s(U - c)^2\tilde{v}_y - [sU'(U - c) + (s - 1)\tilde{g} + \tilde{\alpha}c^2]\tilde{v} = 0, \qquad \text{at } y = 0, \tag{2.1b}$$

$$\tilde{v}_y/\tilde{v} \to -\tilde{\alpha} \qquad \text{as } y \to \infty, \tag{2.1c}$$

where s is the density ratio of air to water, taken to be 10^{-3} in the calculations. The azimuthal angle is related to the wave vector by $\alpha = \tilde{\alpha}\cos\theta$, $\beta = \tilde{\alpha}\sin\theta$, and the solutions are even functions of θ.

The wind velocity profiles in the basic state are adaptations of the mean flow in a turbulent boundary layer, $U(y) = (u_\star/\kappa)[\log(u_\star y/\nu) + A]$, that are defined at $y = 0$. Two are 'lin-log' profiles incorporating a viscous sublayer in which the velocity varies linearly,

$$U(y) = \begin{cases} u_\star^2 y/\nu, & y < y_1 \\ (u_\star/\kappa)[\sinh^{-1}(\kappa u_\star(y - y_1)/\nu) + A - \log(2\kappa)], & y \geqslant y_1, \end{cases} \tag{2.2a}$$

$$U(y) = \begin{cases} u_\star^2 y/\nu, & y < y_1 \\ u_\star^2 y_1/\nu + (u_\star/\kappa)[\gamma - \tanh(\gamma/2)], & y \geqslant y_1, \end{cases} \tag{2.2b}$$

where ν is the kinematic viscosity of air (taken to be 1.5×10^{-5} m^2 s^{-1}), $u_\star$ is the friction velocity, κ is von Kármán's constant (taken to be 0.41), A is the roughness constant (taken to be 2.3), y_1 is the transition height between the linear and logarithmic sections of the profile, and γ is defined by $\sinh(\gamma) = 2u_\star\kappa(y - y_1)/\nu$. The transition height is determined by the requirement that U and its first two derivatives are continuous at $y = y_1$. Two profiles without a linear section have also been examined:

$$U(y) = (u_\star/\kappa)[\log(u_\star y/\nu + 1/\kappa) + A], \tag{2.3a}$$

$$U(y) = (u_\star/\kappa)[\log(u_\star y/\nu + \exp(-A)) + A]. \tag{2.3b}$$

The first has the appropriate slope at $y = 0$, but has non-zero velocity, whilst the second has zero velocity, but incorrect slope. The results presented in §4 are insensitive to the choice of profile, i.e. they do not depend on the details of the basic state near the water surface.

When lengths are scaled by $1/\tilde{\alpha}$ and velocities are scaled by $\tilde{c}_0(\tilde{\alpha}) = [(1 - s)\tilde{g}/(1 + s)\tilde{\alpha}]^{1/2}$, the value of c in the absence of a wind, solutions to the associated two-dimensional problem depend on the two non-dimensional parameters $\tilde{c}_0(\tilde{\alpha})/u_\star$ and $\tilde{\alpha}\nu/u_\star$. In particular,

$$\sigma_{2D} = \tilde{\alpha}\tilde{c}_0(\tilde{\alpha})F\left(\frac{\tilde{c}_0(\tilde{\alpha})}{u_\star}, \frac{\nu\tilde{\alpha}}{u_\star}\right),$$

and hence by Squire's transformation

$$\sigma_{3D} = \alpha\tilde{c}_0(\tilde{\alpha})F\left(\frac{\tilde{c}_0(\tilde{\alpha})}{u_*}, \frac{\nu\tilde{\alpha}}{u_*}\right) = \tilde{\alpha}c_0(\tilde{\alpha})F\left(\frac{c_0(\tilde{\alpha})}{u_*\cos\theta}, \frac{\nu\tilde{\alpha}}{u_*}\right), \tag{2.4}$$

where $c_0(\tilde{\alpha}) = [(1-s)g/(1+s)\tilde{\alpha}]^{1/2}$ is the phase speed of a wave of wavenumber $\tilde{\alpha}$ under the influence of physical gravity. However, it is more illuminating to present the results in terms of wavelength, azimuthal angle, and friction velocity, or equivalently, mean wind speed at ten metres, U_{10}.

3. The occurrence of double-peaked growth rates

The occurrence of growth rates that are double-peaked functions of azimuthal angle when the wavelength is fixed is possible because of the re-scaling of gravity in Squire's transformation. To demonstrate this, a re-scaled friction velocity and wavenumber are defined by $\hat{u}_* = u_*\cos^{2/3}\theta$ and $\hat{\alpha} = \tilde{\alpha}\cos^{2/3}\theta$. When these substitutions are made, the expression for the growth rate (2.4) becomes

$$\sigma_{3D} = \frac{\hat{\alpha}c_0(\hat{\alpha})}{\cos^{1/3}\theta}\,F\left(\frac{c_0(\hat{\alpha})}{\hat{u}_*}, \frac{\nu\hat{\alpha}}{\hat{u}_*}\right),$$

i.e. $\sigma = \hat{\sigma}/\cos^{1/3}\theta$, where $\hat{\sigma}$ is the growth rate of a wave of wavenumber $\hat{\alpha}$, travelling in the direction of a wind of friction velocity $\hat{u}_*$. As θ increases from zero with $\tilde{\alpha}$ fixed, the growth rate, σ_{3D}, is subject to two influences: the factor $\cos^{-1/3}\theta$ acts to increase σ_{3D}, while $\hat{\sigma}$ can act to increase or decrease σ_{3D}. The dependence of $\hat{\sigma}$ on wavelength and friction velocity has been obtained from the series of plots of growth rate against wavelength shown in figure 4 of Morland & Saffman, or more precisely, the portions of those plots for which the critical-layer is above the viscous sublayer. At fixed friction velocity the dimensional growth rate decreases with decreasing wavenumber. However, when the wavenumber is fixed and the friction velocity is decreasing, the growth rate is decreasing for long waves and increasing for short waves. Here, both $\hat{u}_*$ and $\hat{\alpha}$ are decreasing as θ increases, and hence double-peaked growth rates are most likely to occur for shorter waves, when both the decreasing friction velocity and the factor of $\cos^{-1/3}\theta$ act against the decreasing wavenumber.

4. Results

Figure 1(*a*) shows plots of scaled growth rate against azimuthal angle for wavelengths $\lambda = 1$, 3, and 5 m when $u_* = 0.1$ m s^{-1} and $U_{10} = 3.3$ m s^{-1}. At each wavelength the growth rates are scaled by the growth rate at zero azimuthal angle, σ_0, which takes the values 4.9×10^{-4}, 3.7×10^{-5}, and 5.6×10^{-7} s^{-1} at 1, 3, and 5 m. The ratio of the phase speed to the friction velocity, c/u_*, takes the values 12.5, 21.6, and 27.9, respectively, and the scaled wavenumber, $\nu\tilde{\alpha}/u_*$, takes the values 9.4×10^{-4}, 3.1×10^{-4}, and 1.9×10^{-4}. The phase speed has been computed from

$$c = \left(\frac{\lambda(1-s)g}{2\pi(1+s)}\right)^{1/2}.$$

At each wavelength, it can be seen that there is an angle interval in which most of the energy transfer from the wind occurs, the width of which decreases as the wavelength increases. Outside this interval, growth rates are positive, but they are negligible in comparison with a typical growth rate in the interval. The peaks are

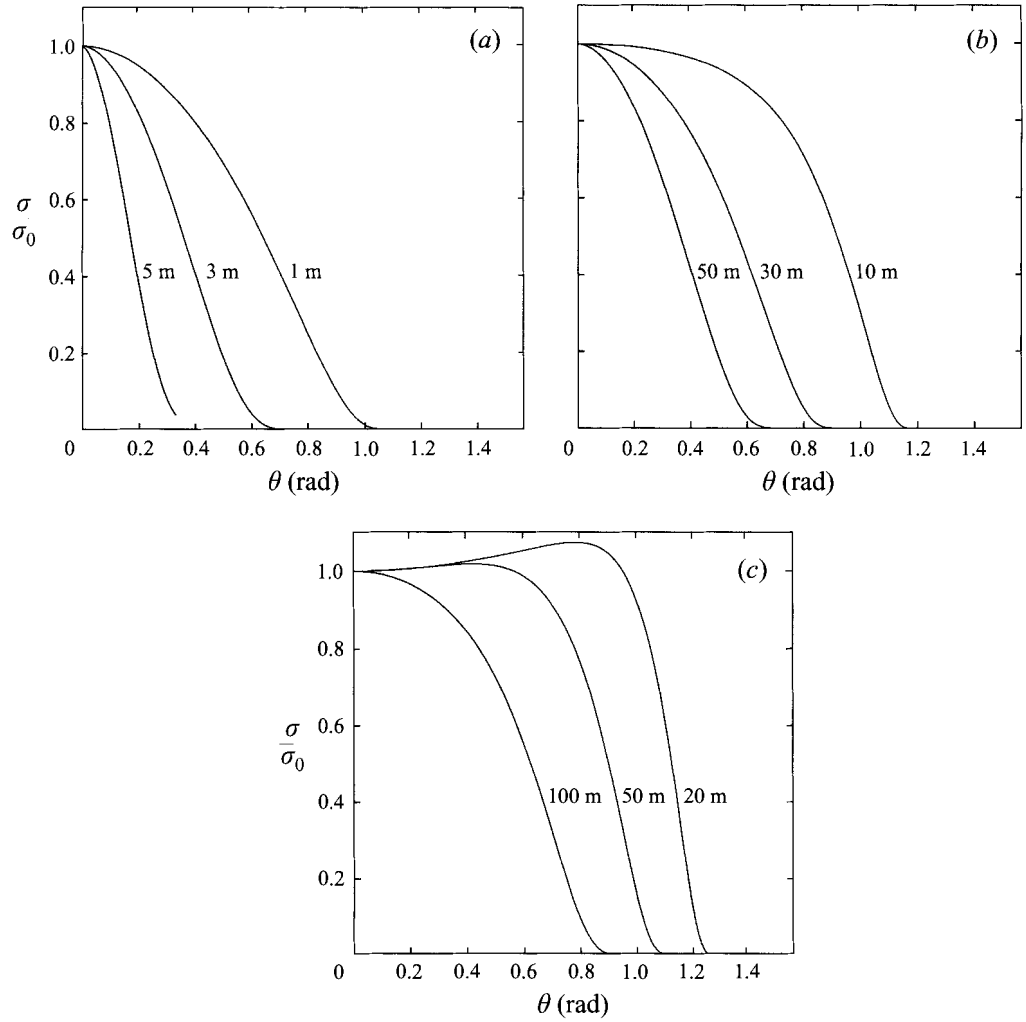

FIGURE 1. Growth rate, scaled by growth rate in the wind direction, against azimuthal angle at fixed wavelength. (*a*) $U_{10} = 3.3$ m s^{-1} ($u_* = 0.1$ m s^{-1}), $\lambda = 1$, 3, and 5 m. (*b*) $U_{10} = 10.6$ m s^{-1} ($u_* = 0.3$ m s^{-1}), $\lambda = 10$, 30, and 50 m. (*c*) $U_{10} = 18.3$ m s^{-1} ($u_* = 0.5$ m s^{-1}), $\lambda = 20$, 50, and 100 m.

coincident with the wind direction. The growth rates shown in figure 1(*a*), and in the other figures, are independent of the choice of profile; disagreement between profiles occurs, at shorter wavelengths than those shown, when the critical layer is low enough that the profiles differ significantly.

As was noted in the introduction, the angular interval of substantial growth rate predicted by the instability is in good agreement with the intervals of positive growth rate given by the summary of field data and by van Duin & Janssens' formula. In the latter two cases, the sign of the growth rate is determined by a factor in the formula in the form $(V\cos\theta - c)/c$, where V is a measure of the wind speed (the speed at a height of 5 m in the case of the field data and at a height of $1/\tilde{\alpha}$, where $\tilde{\alpha}$ is the wavenumber, in the case of van Duin & Janssens' formula). Hence, the width of the interval is determined by V/c, or equivalently c/u_*, and has little or no dependence on $\nu\tilde{\alpha}/u_*$.

When viscous attenuation is included by adding the damping term $-2\nu\tilde{\alpha}^2$ to the

growth rate (Lamb 1945), the growth rates at the lowest wind speed considered here, $U_{10} = 3.3$ m s^{-1}, are small enough that they are significantly reduced.

Results for $u_* = 0.3$ m s^{-1} and $U_{10} = 10.6$ m s^{-1} are shown in figure 1(*b*), for wavelengths of 10, 30, and 50 m, with corresponding values of σ_0 of 1.0×10^{-4}, 2.8×10^{-5}, and 7.6×10^{-6} s^{-1} ($c/u_* = 13.2, 22.8, 29.4$; $\nu\tilde{\alpha}/u_* = 3.1 \times 10^{-5}, 1.0 \times 10^{-5}, 6.3 \times 10^{-6}$). Figure 1(*c*) shows results for $u_* = 0.5$ m s^{-1} and $U_{10} = 18.3$ m s^{-1}, for wavelengths of 20, 50, and 100 m, with corresponding values of σ_0 of 4.4×10^{-5}, 2.3×10^{-5}, and 1.3×10^{-5} s^{-1} ($c/u_* = 11.2, 17.6, 25.0$; $\nu\tilde{\alpha}/u_* = 9.4\times10^{-6}, 3.8\times10^{-6}, 1.9\times10^{-6}$). At $U_{10} = 10.6$ m s^{-1} the growth rate peak is still coincident with the wind direction, but at $U_{10} = 18.3$ m s^{-1} the growth rate is double-peaked at the shorter wavelengths.

Double-peaked growth rates are obtained at the wind speeds of figures 1(*a*) and 1(*b*) if the wavelength is sufficiently short and the profile is of lin-log type. In the case of figure 1(*a*), double-peaked growth rates appear at $\lambda \approx 0.4$ m, and in the case of figure 1(*b*), at $\lambda \approx 5$ m. The growth rate is also double-peaked for the lin-log profiles in the case of the bimodal directional distribution shown by Donelan *et al.* in figure 28(*d*) ($U_{10} \approx 13$ m s^{-1} and $\lambda \approx 6$ m). The peaks in the growth rate are located further from the wind direction than the peaks in the spectrum, but the significance of this result is questionable, since growth rates are sensitive to profile choice at this wind speed and wavelength.

Phillips (1958) presents some bimodal directional distributions in his figure 1 for a friction velocity, assuming a logarithmic velocity profile, of approximately 0.3 m s^{-1}. The directional distribution is bimodal for wavelengths of approximately 64 m and less; the smallest wavelength shown is 44 m. The data presented here in figure 1(*b*) indicate that these bimodal distributions cannot be attributed to the instability being studied here, and Phillips presents evidence that his resonance mechanism (Phillips 1957) is responsible. For a wave of wavenumber $\tilde{\alpha}$, the resonant wave generation mechanism predicts peaks at $\pm\theta$ if $c/U < 1$, where U is the wind speed at height $1/\tilde{\alpha}$, c is the phase speed of the wave, θ is the angle to the wind of the direction of propagation, and $U\cos(\theta) = c$. If $c/U \geqslant 1$, the peak is in the direction of the wind. Jackson *et al.* present directional distributions for wavelengths ranging from 74 m to 220 m, at a wind speed of about 11 m s^{-1}. Those with wavelengths between 86 m and 129 m are bimodal and the locations of the peaks in the directional distributions are in agreement with Phillips' resonance mechanism. Once again, figure 1(*b*) indicates that the bimodal distributions are not connected with the instability.

The spectra of Donelan *et al.* and Jackson *et al.* differ greatly in the peak angular frequency of the spectrum, which is $\omega_p = 2.31$ s^{-1} in the former case and $\omega_p = 0.75$ s^{-1} in the latter. There is also a difference in the part of the spectrum in which the bimodal directional distributions appear. The bimodal distribution observed by Donelan *et al.* is at $\omega/\omega_p = 1.4$, while Jackson *et al.* observe bimodal distributions for ω/ω_p between 0.92 and 1.13.

The figures discussed above indicate that the width of the unstable interval increases with increasing wind speed, and this is confirmed in figure 2, which shows plots of dimensional growth rate against azimuthal angle for a 30 m wave when $U_{10} = 10.6$, 14.4, and 22.2 m s^{-1} ($c/u_* = 22.8, 17.1, 11.4$, $\nu\tilde{\alpha}/u_* = 1.0\times10^{-5}, 7.9\times10^{-6}, 5.2\times10^{-6}$). Below the lowest wind speed shown, growth rates decrease rapidly with wind speed, as the critical layer rises into a region of very low profile curvature, and above the highest wind speed shown growth rates start to depend on profile choice, as the critical layer descends towards the viscous sublayer. At a fixed wind speed, when the growth rate is double-peaked, the peaks move apart with decreasing wavelength,

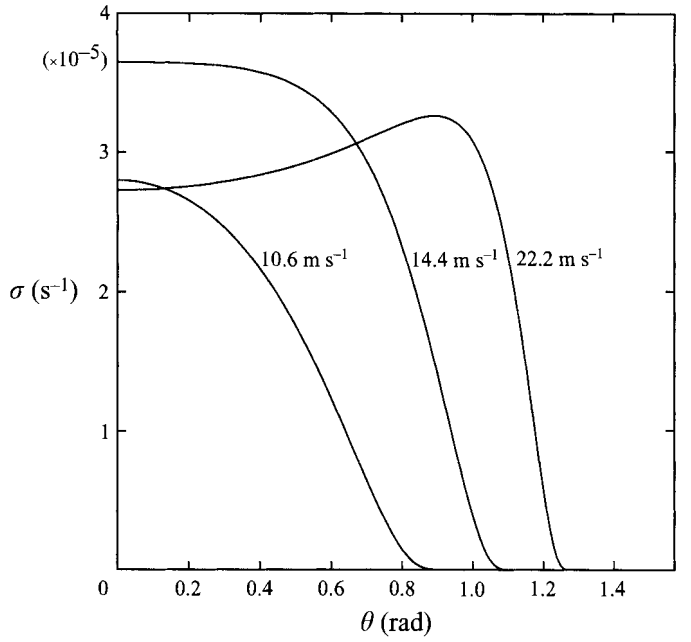

FIGURE 2. Growth rate against azimuthal angle for a wave of length 30 m when $U_{10} = 10.6$, 14.4, and 22.2 m s^{-1} ($u_* = 0.3$, 0.4, and 0.6 m s^{-1}).

as also occurs in the case of Phillips' resonance mechanism. However, for a given wind, the resonance mechanism predicts peaks that are further apart than those of the instability, since they are located at the ends of the angle interval over which the instability is effective.

Figure 3 shows the dividing lines between double-peaked and single-peaked growth rates in the $(c/u_*, \nu\tilde{\alpha}/u_*)$-plane computed from a lin-log profile (2.2a) and a logarithmic profile (2.3a). Single-peaked growth rates occur above the dividing lines and double-peaked below. The region in which the inviscid instability is important is given approximately by $c/u_* > 8$, and the two profiles give consistent, and hence most convincing, results when $c/u_* > 12$.

Young *et al.* show directional distributions at six wind speeds. In all cases except one, the bimodal distributions occur at parameter values for which either the neglect of viscosity in the stability analysis is not justified ($c/u_* < 8$) or the two profile types give inconsistent results. In the exceptional case, $c/u_* \approx 10$ and $\nu\tilde{\alpha}/u_* \approx 4 \times 10^{-4}$, the inviscid instability exhibits a single-peaked growth rate. Hence, it is not clear whether the inviscid instability contributes to the bimodal distributions or not.

The growth rates computed from van Duin & Janssens' formula are of the same order of magnitude as those of the critical-layer mechanism for the parameter values discussed above. At a constant friction velocity, van Duin & Janssens' growth rates decrease more rapidly with increasing wavelength; comparing with the data of figure 1, they are smaller at the three wavelengths and are negative for the largest wavelength, $\lambda = 5$ m. At a fixed wavelength, van Duin & Janssens' growth rates increase monotonically with increasing friction velocity, while as can be seen in figure 2, those associated with the critical layer do not. In the cases of double-peaked growth rates shown above, van Duin & Janssens's maximum growth rates over angle to the wind are larger by a factor of approximately two.

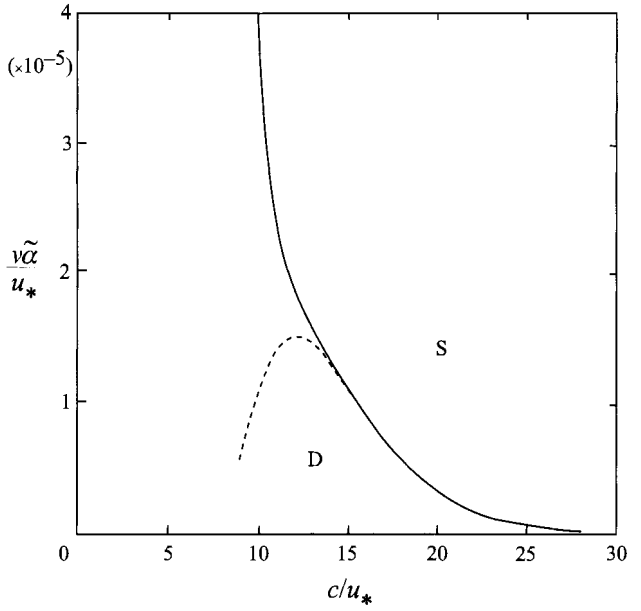

FIGURE 3. The dividing line in the $(c/u_*, \nu\tilde{\alpha}/u_*)$-plane between single-peaked and double-peaked growth rates when the wind is of lin-log type (solid line) and of logarithmic type (dashed line). Single-peaked growth rates (S) occur above the dividing lines and double-peaked (D) occur below.

5. Summary and concluding remarks

For a wind of 'lin-log' type, the energy transfer to the waves due to the inviscid critical-layer mechanism is largely concentrated in an angle (to the wind) interval $[-\theta, \theta]$ that broadens with increasing wind speed and narrows with increasing wavelength. An empirical formula for θ is $\cos\theta = c/V$, where c is the wave speed and V is the wind speed at the reciprocal of the wavenumber.

Observations in the field provide evidence that bimodal directional distributions occur at sea. Several mechanisms appear, in isolation, to be capable of giving rise to bimodal directional distributions: the resonant wave generation mechanism, wave–wave interactions, wave scattering, and as demonstrated here, the inviscid critical-layer mechanism. The relative importance of these mechanisms and how they interact in the formation of the spectrum are open questions, but it seems reasonable to look for the influence of energy input from the wind at frequencies away from the peak frequency, where the nonlinear mechanisms will have least influence.

For a given wind, the inviscid critical-layer mechanism predicts double-peaked growth rates as a function of angle to the wind at the shortest wavelengths at which it acts. This prediction is most convincing at the higher wind speeds that occur at sea, for which the double-peaked growth rates are insensitive to the form of the wind profile near the water surface. Both the resonant wave generation mechanism and wave–wave interactions have been connected with observed bimodal directional distributions, but at present there is only a very tentative connection between the inviscid critical-layer mechanism and an observed bimodal directional distribution.

REFERENCES

BANNER, M. L. & MELVILLE, W. K. 1976 On the separation of air flow over water waves. *J. Fluid Mech.* **77**, 825–842.

BELCHER, S. E. & HUNT, J. C. R. 1993 Turbulent shear flow over slowly moving waves. *J. Fluid Mech.* **251**, 109–148.

BENJAMIN, T. B. 1959 Shearing flow over a wavy boundary. *J. Fluid Mech.* **6**, 161–205.

BURGERS, G. & MAKIN, V. K. 1993 Boundary-layer model results for wind-sea growth. *J. Phys. Oceanogr.* **23**, 372–385.

COTÉ, L. J., DAVIS, J. O., MARKS, W. *et al.* 1960 The directional spectrum of a wind generated sea as determined from data obtained by the Stereo Wave Observation Project. *New York University College of Engineering, Meteorol. Paper,* 2, No. 6, 88 pp.

DONELAN, M. A., HAMILTON, J. & HUI, W. H. 1985 Directional spectra of wind-generated waves. *Phil. Trans. R. Soc. Lond.* A **315**, 509–562.

DUIN, C. A. VAN & JANSSEN, P. A. E. M. 1992 An analytical model of the generation of surface gravity waves by turbulent air flow. *J. Fluid Mech.* **236**, 197–215.

JACKSON, F. C., WALTON, W. T. & PENG, C. Y. 1985 A comparison of in situ and airborne radar observations of ocean wave directionality. *J. Geophys. Res.* **90** (C1), 1005–1018.

JACOBS, S. J. 1987 An asymptotic theory for the turbulent flow over a progressive water wave. *J. Fluid Mech.* **174**, 69–80.

KNIGHT, D. 1977 Turbulent flow over a wavy boundary. *Boundary-Layer Met.* **11**, 205–222.

LAMB, H. 1945 *Hydrodynamics*, 6th edn. Dover.

MILES, J. W. 1957 On the generation of surface waves by shear flows. *J. Fluid Mech.* **3**, 185–204.

MILES, J. W. 1962 On the generation of surface waves by shear flows. Part 4. *J. Fluid Mech.* **13**, 433–448.

MILES, J. W. 1993 Surface-wave generation revisited. *J. Fluid Mech.* **256**, 427–441.

MITSUYASU, H., TASAI, F., SUHARA, T. *et al.* 1975 Observations of the directional spectrum of ocean waves using a cloverleaf buoy. *J. Phys. Oceanogr.* **5**, 750–760.

MORLAND, L. C. & SAFFMAN, P. G. 1993 Effect of wind profile on the instability of wind blowing over water. *J. Fluid Mech.* **252**, 383–398.

PHILLIPS, O. M. 1957 On the generation of waves by turbulent wind. *J. Fluid Mech.* **2**, 417–445.

PHILLIPS, O. M. 1958 On some properties of the spectrum of wind-generated ocean waves. *J. Mar. Res.* **16**, 231–245.

PHILLIPS, O. M. 1977 *The Dynamics of the Upper Ocean*, 2nd edn. Cambridge University Press.

PHILLIPS, O. M. 1988 Remote sensing of the sea surface. *Ann. Rev. Fluid Mech.* **20**, 89–109.

SNYDER, R. L., DOBSON, F. W., ELLIOTT, J. A. & LONG, R. B. 1981 Array measurements of atmospheric pressure fluctuations above surface gravity waves. *J. Fluid Mech.* **102**, 1–59.

VALENZUELA, G. R. 1976 The growth of gravity-capillary waves in a coupled shear flow. *J. Fluid Mech.* **76**, 229–250.

YOUNG, I. R., VERHAGEN, L. A. & BANNER, M. L. 1995 A note on the bimodal directional spreading of fetch-limited wind waves. *J. Geophys. Res.* **100** (C1), 773–778.

ZAKHAROV, V. E. & SHRIRA, V. I. 1990 Formation of the angular spectrum of wind waves. *Sov. Phys. JETP* **71**, No. 6, 1091–1100.